A&A 383, 653–660 (2002)
DOI: 10.1051/0004-6361:20011759

Astronomy & Astrophysics

Models for solar magnetic loops

I. A simple theoretical model and diagnostic procedure

M. Landini[1] and E. Landi[2,3]

[1] Dipartimento di Astronomia e Scienza dello Spazio, Università di Firenze, Italy
[2] Max-Planck-Institut für Aeronomie, Katlenburg-Lindau, Germany
[3] Naval Research Laboratory, Washington DC, 20375-5320, USA

Received 27 October 2000 / Accepted 28 November 2001

Abstract. In the present paper the quasi-static model of Landini & Monsignori Fossi (1975) for coronal loops is improved and a simple diagnostic procedure is developed to compare the most important physical properties of the model with a set of spectral observations of loops such as those obtained by the CDS and SUMER instruments on SOHO. The model assumes quasi-static and isobaric conditions and solves the energy equation among radiative losses, a constant heating function and heat conduction. The model is allowed to have a variable loop section. To better match the latest observational results, an isothermal section of the loop is added at the top of the loop model; its effects on the diagnostic technique and on the shape of the unknown heating function are discussed. A numerical simulation is shown and the effect of the isothermal region is discussed. In a second paper (Brković et al. 2002, Paper II) the present model will be compared with observations from the SOHO satellite.

Key words. Sun: corona – techniques: miscellaneous

1. Introduction

The first attempts to model loop structures in the solar corona date back to the 1970s following from the large number of broad-band X-ray pictures obtained by Skylab. One of the first models was published by one of the authors with the aim of predicting the X-ray emission from stellar coronae (Landini & Monsignori Fossi 1973), and was successively developed to allow comparison with solar observations (Landini & Monsignori Fossi 1975). This model was based on the solution of the energy balance among radiative losses, energy input and conductive energy in a constant-section, stationary and static loop. This model also allowed one to introduce the *scaling laws*, simple relations that involve the most relevant physical quantities of the loop.

A few years later Rosner et al. (1978, hereafter RTV) improved the Landini & Monsignori Fossi (1975) model using a better approximation to the radiative losses versus temperature function and investigating different mechanisms of power supply. Extensive use has been made in the last twenty years of the RTV scaling laws (especially involving the loop length), by applying them to coronal loop observations from the Solar Maximum Mission (SMM, Solar Physics 1980) and Yohkoh (Ogawara et al. 1991). A more general hydrostatic model including also the effects of subsonic velocity and gravity has been developed by the same authors (Landini & Monsignori Fossi 1981) and different shapes of the power supply versus temperature are discussed there. The RTV model has been extended to include velocity fields and the effect of gravity (Serio et al. 1981; Orlando et al. 1995a,b; see also the review of Peres 1997).

Most of the solar missions launched in the last twenty years and devoted to the study of the solar corona have produced images of the Sun with increasingly better spatial resolution, using broad band detectors. The main limitation of these instruments (SMM, Yohkoh) was the rather poor spectral resolution. Recently, the launch of the SOHO and TRACE satellites, carrying several instruments devoted to the investigation of the chromosphere, transition region and corona, has allowed detailed comparisons between theoretical loop models and observations.

Despite all the efforts, however, loop models are still unable to adequately explain the observations, the processes that heat the plasma inside loops have not been understood, and no conclusion has been reached on the shape of the loop heating function.

The aim of the present work is multiple:

1. to extend the loop model originally developed by Landini & Monsignori Fossi (1975), including the most

Send offprint requests to: E. Landi,
e-mail: landi@poppeo.nrl.navy.mil

recent calculation of radiative losses, and a variable cross-section;
2. to discuss the joining of an isothermal region at the top of the loop and the effects of high conductive fluxes at the base;
3. to present a new, simple diagnostic procedure to evaluate the most relevant physical properties of a loop by comparing model predictions and monochromatic observations;
4. to carry out a thorough comparison with broad band images of an active region loop system, taken with the SOHO-EIT and Yohkoh-SXT satellites, and with monochromatic images from spectral line intensities observed with the CDS instrument.

For this reason, this work has been divided in two separate papers: the present (Paper I) describes the improved loop model and the diagnostic technique, and discusses the inclusion of an isothermal portion of the loop and its consequences on the diagnostic technique. The accompanying paper (Brković et al. 2002, Paper II) will describe the comparison of the model with the observations and report the main physical quantities of the observed loops.

The present paper is structured as follows: Sect. 2 illustrates the theoretical model, both in its analytical and in its numerical form. Section 3 describes the diagnostic technique and Sect. 4 discusses the inclusion of an isothermal section of the loop and its consequences for the heating function, and the presence of the conductive flux at the base of the loop. Section 5 summarizes the conclusions.

2. The theoretical model and diagnostic technique

The present loop model is based on the following five assumptions:

- Steady-state conditions,
- Hydrostatic equilibrium,
- Negligible velocities,
- Constant pressure (p_0),
- Uniform heating function.

The first assumption is common to most of the loop models in the literature. TRACE observations however show that in many cases coronal loops seem to undergo strong variability: see for example the results on a brightening coronal loop obtained by Reale et al. (2000a,b). Similar results, obtained with SOHO-CDS, show that coronal loops are relatively stable in time, while the highest time variability occurs to loops with $T < 5 \times 10^5$ K (Kjeldseth-Moe & Brekke 1998). However, this assumption has been criticized by Aschwanden et al. (1999, 2000a) and will be discussed later. Aschwanden et al. (1999, 2000a) also find that coronal loops are in hydrostatic equilibrium. Plasma flows have been observed on active region loops; measured speeds rise up to more than 50 km s^{-1} for cold loops, but do not exceed $\simeq$15 km s^{-1} for coronal loops (Spadaro et al. 2000). Since the sound speed in a coronal loop with $T \simeq 10^6$ K is around 150 km s^{-1}, the negligible-velocity assumption is realistic. The constant pressure assumption is taken here for simplicity, but for loops higher than the scale height H it does not hold. For coronal plasma with $T \simeq 2 \times 10^6$ K, H is around 10^5 km, comparable with the coronal loop lengths. In Paper II it is shown that this assumption holds for the loop studied in the present work. However the main effect of gravity is to deplete and reduce the emission of the loop top, an effect that can be easily detected on the images, and can be easily verified with line ratio techniques. The uniform heating function assumption has been criticized by Aschwanden et al. (2000b, 2001), and will be discussed in Sect. 4.

Constant and physical quantities are always expressed in cgs units throughout the remainder of the paper.

In this paper attention is focused on the development of the Landini & Monsignori Fossi (1975) model, based on the above five assumptions, so that the whole model rests on two parameters only (see Sects. 2.1 and 2.2) and allows the development of a straightforward diagnostic technique. A future work will generalize the model following the Landini & Monsignori Fossi (1981) model.

The energy balance equation, per unit volume and time, in the static approximation may be expressed as

$$E_\mathrm{i} - E_\mathrm{r} - E_\mathrm{c} = 0 \tag{1}$$

where E_r indicates radiative losses, E_i represents the (unknown) energy input and E_c indicates energy conduction by free electrons.

We first describe an analytical model which helps in defining the basic relations and scaling laws for the loop; a more accurate, numerical model will be developed in Sect. 2.2.

2.1. The analytical model

In order to carry out the analytical solution of the model, we assume a simple analytical form for the radiative losses:

$$E_\mathrm{r} = -C\frac{p_0^2}{T^{2.5}} \qquad C \simeq 2 \times 10^{12}\ \mathrm{K}^{\frac{5}{2}}\ \mathrm{cm}^3\ \mathrm{s}^{-1}\ \mathrm{erg}^{-1}. \tag{2}$$

This analytical form reasonably reproduces the radiative losses calculated by Landi & Landini (1999). If we define T_M as the temperature where radiative losses are equal to the energy input, the conductive energy $E_\mathrm{c} = 0$, and the conductive flux F_c reaches its maximum value, we have:

$$E_\mathrm{i} = E_\mathrm{r}(T_\mathrm{M}) = \text{constant}; \qquad E_\mathrm{c}(T_\mathrm{M}) = 0. \tag{3}$$

Adopting the expression for the conductive flux

$$F_\mathrm{c} = -AT^{5/2}\,\frac{\mathrm{d}T}{\mathrm{d}h}$$
$$A = 0.92 \times 10^{-6}\ \mathrm{K}^{-3.5}\ \mathrm{erg\ cm}^{-1}\ \mathrm{s}^{-1} \tag{4}$$

with A from Spitzer (1962), we can express E_c as

$$E_\mathrm{c} = -\frac{\mathrm{d}F_\mathrm{c}}{\mathrm{d}h} = -\frac{\mathrm{d}F_\mathrm{c}}{\mathrm{d}T}\frac{\mathrm{d}T}{\mathrm{d}h} = \frac{\mathrm{d}F_\mathrm{c}}{\mathrm{d}T}\ \frac{F_\mathrm{c}}{AT^{5/2}} \tag{5}$$

where h is the length along the loop. Using the above equations we can write

$$F_{\rm c}\ \frac{{\rm d}F_{\rm c}}{{\rm d}T} = A\ T^{5/2}\left(\frac{Cp_0^2}{T^{2.5}} - \frac{Cp_0^2}{T_{\rm M}^{2.5}}\right). \tag{6}$$

Introducing the reduced variables

$$t = \frac{T}{T_{\rm M}} \qquad f = \frac{F_{\rm c}}{F_0} \qquad F_0^2 = CAp_0^2T_{\rm M}. \tag{7}$$

Equation (6) may be re-written as

$$f\ {\rm d}f = \left(\frac{1}{t^{2.5}} - 1\right)t^{2.5}{\rm d}t \tag{8}$$

and can easily be integrated:

$$\int_{f_1}^{f} f\ {\rm d}f = \int_{t_1}^{t}\left(1 - t^{5/2}\right){\rm d}t \quad \Longrightarrow$$
$$\frac{f^2}{2} = \frac{f_1^2}{2} + \left(t - \frac{2}{7}t^{7/2}\right) - \left(t_1 - \frac{2}{7}t_1^{7/2}\right). \tag{9}$$

The lower limit of the integral is needed because the approximation used for $E_{\rm r}$ in Eq. (2) is valid only for temperatures larger than 10^5 K ($t > t_1 = 10^5/T_{\rm M}$). f_1 is the conductive flux of the loop at temperature t_1, typical of the lower transition region.

The scaled coronal top temperature $t_{\rm top}$ is reached when $f = 0$. For negligible f_1 and t_1 we obtain

$$f = -\sqrt{2}\left(t - \frac{2}{7}t^{7/2}\right)^{1/2} \quad \Longrightarrow$$
$$t_{\rm top} = \left(\frac{7}{2}\right)^{2/5} = 1.65. \tag{10}$$

However, this result is only indicative, since the assumption that the conductive flux vanishes at $T = 10^5$ K is very crude. If proper values of f_1 are evaluated following the same procedure for $t < t_1$ and using a more accurate representation for the radiative losses at T smaller than 10^5 K, $t_{\rm top}$ changes; a more accurate value is

$$t_{\rm top} = 1.25 \quad \Longrightarrow \quad T_{\rm top} = 1.25 \times T_{\rm M}. \tag{11}$$

Using the standard definitions in the literature, we define the Emission Measure (*EM*) and the Differential Emission Measure (*DEM*) as

$$DEM = N_{\rm e}^2\frac{{\rm d}V}{{\rm d}T} \tag{12}$$

$$EM = \int_V N_{\rm e}^2{\rm d}V = \int_T DEM(T){\rm d}T. \tag{13}$$

Assuming that the loop has constant cross-section S and constant pressure p_0 we have ${\rm d}V = S\ {\rm d}h$

$$DEM = S\ N_{\rm e}^2\frac{{\rm d}h}{{\rm d}T} = \frac{Sp_0^2}{4k^2}\frac{1}{T^2}\frac{{\rm d}h}{{\rm d}T}. \tag{14}$$

The quantity $\frac{{\rm d}h}{{\rm d}T}$ is related to the conductive flux from Eq. (4) so that we can express the *EM* over the temperature interval $[t_i,t_{i+1}]$ as

$$EM = \int_V N_{\rm e}^2{\rm d}V = \frac{Sp_0}{4k^2}T_{\rm M}\sqrt{\frac{A}{C}}\int_{t_i}^{t_{i+1}} t^{1/2}f^{-1}{\rm d}t \tag{15}$$

where k is the Boltzmann constant. From Eqs. (14) and (15) it is possible to see that the natural scaling unit for the *EM* is $\frac{Sp_0}{4k^2}T_{\rm M}\sqrt{\frac{A}{C}}$, and the natural scaling law for the *DEM* is $\frac{Sp_0}{4k^2}\sqrt{\frac{A}{C}}$.

As long as Eq. (10) holds, the *EM* has the form

$$\int_V N_{\rm e}^2{\rm d}V = \frac{Sp_0}{4k^2}T_{\rm M}\sqrt{\frac{A}{C}}\int_{t_i}^{t_{i+1}}\frac{{\rm d}t}{\sqrt{2}\ \sqrt{\left(1 - \frac{2}{7}t^{5/2}\right)}}. \tag{16}$$

If we scale the *EM* by its natural scaling unit, and change the integration variable according to

$$\cos\theta = \sqrt{\frac{2}{7}\ t^{5/2}} \tag{17}$$

the scaled emission measure can be evaluated according to the relation

$$\int_V N_{\rm e}^2{\rm d}V = \frac{1}{\sqrt{2}}\left(\frac{7}{2}\right)^{\frac{2}{5}}\frac{4}{5}\int_{\theta(t_i)}^{\theta(t_{i+1})}(\cos\theta)^{-\frac{1}{5}}{\rm d}\theta. \tag{18}$$

The largest value of the emission measure assuming ${\rm d}T$ values of $10^{0.1}$ is reached in the temperature interval from $10^{0.1}t_{\rm top}$ to $t_{\rm top}$ and provides the greatest contribution to coronal line intensity. The present change of variables allows one to avoid the divergence of the integrand near the top temperature and to correctly evaluate this very important contribution.

From the knowledge of the conductive flux the length versus temperature $L(T)$ model may be evaluated in a similar way, giving

$$L = \int {\rm d}h = \int \frac{AT^{2.5}}{F}{\rm d}T =$$
$$= \sqrt{\frac{A}{C}}\frac{T_{\rm M}^3}{p_0}\frac{1}{\sqrt{2}}\left(\frac{7}{2}\right)^{\frac{6}{5}}\frac{4}{5}\int_{\frac{\pi}{2}}^{\theta(t)}(\cos\theta)^{\frac{7}{5}}{\rm d}\theta. \tag{19}$$

The well known scaling factor for lengths, $\sqrt{\frac{A}{C}}\frac{T_{\rm M}^3}{p_0}$, is then defined by Eq. (19). The total loop length value is obtained for $\theta = 0$:

$$L = 2.28 \times \sqrt{\frac{A}{C}}\frac{T_{\rm M}^3}{p_0}. \tag{20}$$

2.2. The numerical model

The analytical model of Sect. 2.1 is useful to introduce the scaling laws for the main physical quantities that characterize the model, as conductive flux, scale length, *DEM* and integrated *EM*. However, in order to take into account more accurately the temperature dependence of the radiative losses and to allow for different initial conditions, it is necessary to perform the integration of the energy equation numerically. Moreover, the loop cross-section has been allowed to expand from the footpoints to the loop top. This last change has been made necessary in order to better reproduce the emission of the transition region lines (see Paper II).

Radiative losses from Landi & Landini (1999) have been adopted and scaled according to

$$E_{\rm rad} = C\frac{p_0^2}{T^{5/2}}\varepsilon(T) \tag{21}$$

C has the same value and units of Eq. (2). $E_{\rm rad}/p_0^2$ is displayed in Fig. 1.

The constant loop cross-section assumption commonly adopted in literature is also released, and a variable loop cross-section has been adopted. The geometrical cross-section of the loop S has been parametrized with

$$S = S_{\rm M}\ \sigma(nt)$$
$$\sigma(nt) = \frac{S_{\rm m}}{S_{\rm M}} + \left(1 - \frac{S_{\rm m}}{S_{\rm M}}\right)(\tan h(nt))^5 \tag{22}$$

where $t = \frac{T}{T_{\rm M}}$ is the scaled temperature, $S_{\rm M}$ and $S_{\rm m}$ are the maximum and minimum loop cross-section respectively, and n a number that allows to control the height where the section begins to increase. The $\frac{S_{\rm m}}{S_{\rm M}}$ and n values are selected as those providing the best agreement between theoretical and observed line intensities. The variable loop cross-section assumption is supported by the intensity maps observed with the SOHO instruments (see Paper II): the sizes of the footpoint regions emitting the cooler lines are much smaller than the section of the coronal part of the loop.

With these new definitions, the conductive energy and the energy equation take the form:

$$E_{\rm c} = -\frac{1}{S}\frac{{\rm d}(SF_{\rm c})}{{\rm d}h} = -\frac{1}{S}\frac{{\rm d}(SF_{\rm c})}{{\rm d}T}\frac{{\rm d}T}{{\rm d}h}$$
$$= \frac{1}{S}\frac{{\rm d}(SF_{\rm c})}{{\rm d}T}\ \frac{F_{\rm c}}{AT^{5/2}} \tag{23}$$

$$\frac{F_{\rm c}}{S}\ \frac{{\rm d}(SF_{\rm c})}{{\rm d}T} = A\ T^{5/2}(E_{\rm rad}(T) - E_{\rm i}) \tag{24}$$

where $E_{\rm i} = E_{\rm rad}(T_{\rm M})$. Using the new variable $W = SF_{\rm c}$ and adopting the scaling

$$W = wW_{\rm o} \qquad W_{\rm o}^2 = S_{\rm M}^2 AC p_0^2 T_{\rm M}. \tag{25}$$

The new scaled energy equation becomes:

$${\rm d}w^2 = 2\sigma^2\Big(\varepsilon(t) - \varepsilon(1)t^{5/2}\Big){\rm d}t \tag{26}$$

to be integrated from $w(t_{\rm o}) \simeq 0$ and $t_{\rm o} = \frac{2\times10^4}{T_{\rm M}}$ K. It is important to note that this assumption corresponds to assuming that the loop is thermally isolated from the lower transition region and chromosphere. This assumption is very important, since a change of the quantity $w(t_{\rm o})$ can significantly change the results. Recently Oluseyi et al. (1999) argued that it is more reasonable to assume that the loop is *not* thermally isolated, so that their resulting loop models are significantly different from those in the present work. This issue is discussed in Sect. 4.2.

Once w is known, the dimensionless quantities become:

– conductive flux: $f = \frac{w}{\sigma}$

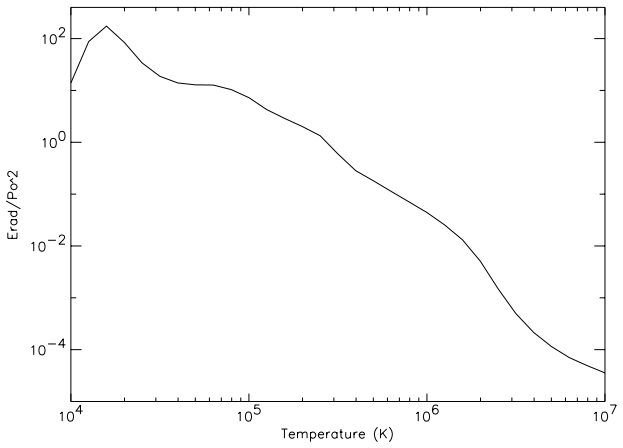

Fig. 1. $E_{\rm rad}/p_0^2$ as a function of electron temperature. Units are erg^{-1} cm^3 s^{-1}.

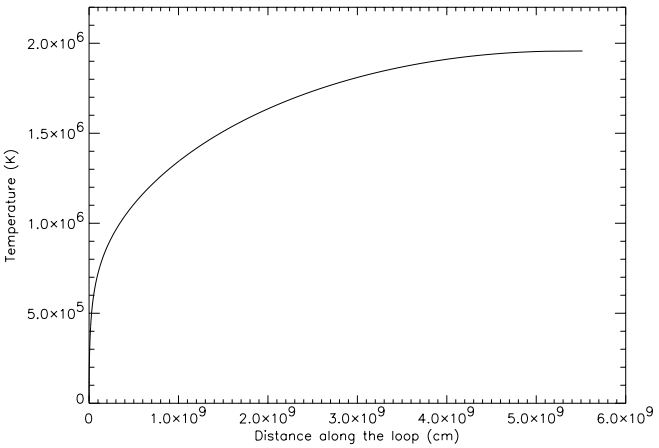

Fig. 2. Typical properties of the theoretical model: temperature versus position along the loop. The model has been calculated assuming Log $T_{\rm M} = 6.1$, $n = 1.6$, $S_{\rm M}/S_{\rm m} = 15$, $p_0 = 1.0$ dyne cm^{-2}.

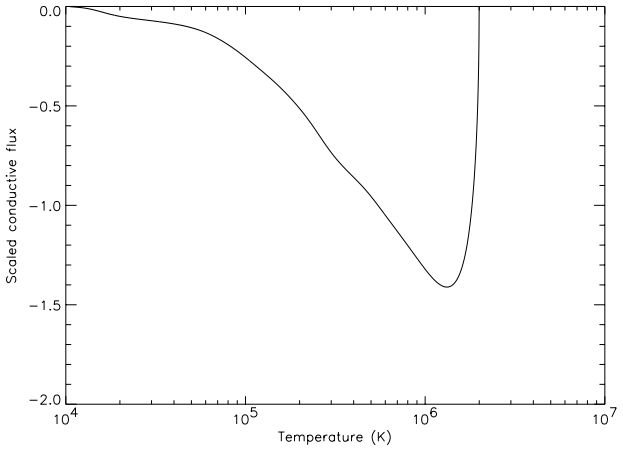

Fig. 3. Typical properties of the theoretical model: conductive flux versus temperature. The model has been calculated assuming Log $T_{\rm M} = 6.1$, $n = 1.6$, $S_{\rm M}/S_{\rm m} = 15$, $p_0 = 1.0$ dyne cm^{-2}.

– Differential Emission Measure: $DEM = \frac{t^{0.5}}{w}\sigma^2$
– Length: $L = \int \frac{t^{2.5}}{w}\sigma{\rm d}t$
– Emission Measure: $EM = \int \frac{t^{0.5}}{w}\sigma^2{\rm d}t$

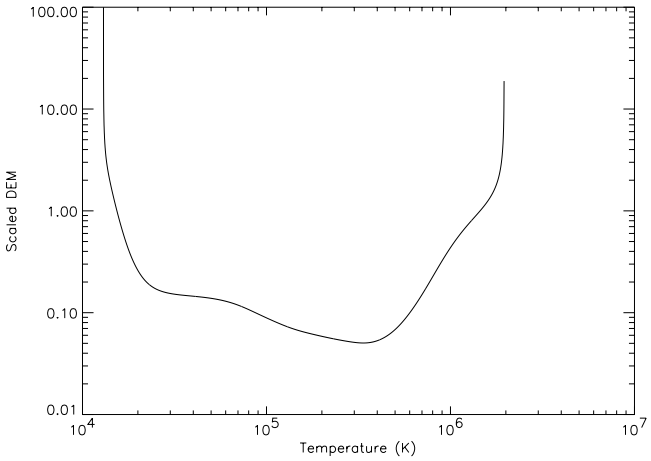

Fig. 4. Typical properties of the theoretical model: *DEM* versus temperature. The model has been calculated assuming Log $T_{\rm M} = 6.1$, $n = 1.6$, $S_{\rm M}/S_{\rm m} = 15$, $p_0 = 1.0$ dyne cm^{-2}.

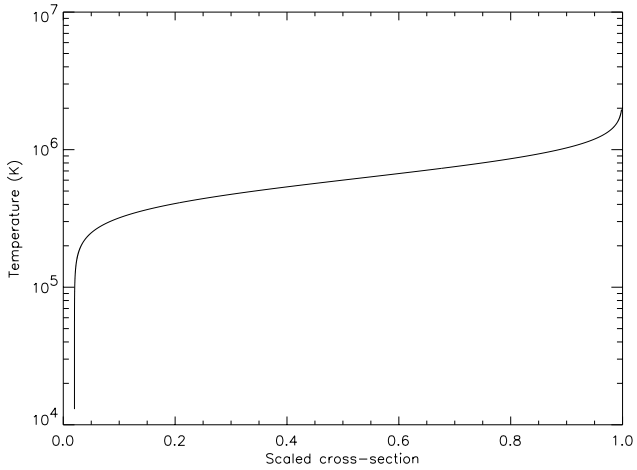

Fig. 5. Typical properties of the theoretical model: example of the function $\sigma(T)$. The model has been calculated assuming Log $T_{\rm M} = 6.1$, $n = 1.6$, $S_{\rm M}/S_{\rm m} = 15$, $p_0 = 1.0$ dyne cm^{-2}.

in the same scaled values as above. The scaling laws resulting from this model are similar to the analytical ones, with the exception of correction factors that are slightly dependent on $T_{\rm M}$. For example, the loop length scaling law takes the form

$$L_{\rm loop} = r(T_{\rm M}) \sqrt{\frac{A}{C}} \frac{T_{\rm M}^3}{p_0} \tag{27}$$

where $r(T_{\rm M})$ is a number near unity which is slightly dependent on $T_{\rm M}$; the loop top temperature is given by

$$t_{\rm top} = c(T_{\rm M}) \quad \Longrightarrow \quad T_{\rm top} = c(T_{\rm M}) \times T_{\rm M} \tag{28}$$

where $c(T_{\rm M})$ typically ranges between 1.0 and 2.0.

Samples of some physical quantities determined by the loop model are shown in Figs. 2 to 5 for Log $T_{\rm M} = 6.1$.

3. The diagnostic technique

The flux received at Earth at distance d in an optically thin spectral line j from a loop modeled according to Sect. 2.2 is given by

$$F_j = \frac{S_{\rm M} p_0}{4k^2} T_{\rm M}^\star \sqrt{\frac{A}{C}} \frac{1}{4\pi d^2} \int G_j(T, N_{\rm e}) \frac{t^{1/2}}{w} \sigma^2(t) {\rm d}t \tag{29}$$

where $G_j(T, N_{\rm e})$ is the Contribution Function of the line j; t, w, σ are the scaled temperature, conductive energy and cross-section of the loop, $S_{\rm M}$ is the maximum cross-section of the loop, p_0 is the total loop pressure, $T_{\rm M}^\star$ is the temperature at which radiative losses equal the energy input in the observed loop. All the quantities are in cgs units. We can define the ratio $R(T_{\rm M})$ as

$$R(T_{\rm M}) = \frac{F_j^{\rm obs}}{J_j(T_{\rm M})} \tag{30}$$

where $F_j^{\rm obs}$ is the observed line flux integrated over the whole loop shape, and $J_j(T_{\rm M})$ is given by

$$J_j(T_{\rm M}) = T_{\rm M} \int_T G_j(T)\ DEM\left(\frac{T}{T_{\rm M}}\right) {\rm d}T \tag{31}$$

$T_{\rm M}$ is the temperature at which radiative losses equal energy input in the theoretical model. For each observed line, the $R(T_{\rm M})$ function can be evaluated and displayed on the same plot as a function of $T_{\rm M}$. It is possible to show that, if the loop model is correct, when $T_{\rm M} = T_{\rm M}^\star$ all the curves assume the same value $R(T_{\rm M}^\star) = \frac{S_{\rm M} p_0}{4k^2} \sqrt{\frac{A}{C}} \frac{1}{4\pi d^2}$, and meet at the point

$$\left(T_{\rm M}^\star, \frac{S_{\rm M} p_0}{4k^2} \sqrt{\frac{A}{C}} \frac{1}{4\pi d^2} \right). \tag{32}$$

Thus, it is possible to determine simultaneously both the value of $T_{\rm M}^\star$ (and hence the loop top temperature) and of $p_0 S_{\rm M}$. An example is given in Fig. 6.

The shape of each $R(T_{\rm M})$ function in Fig. 6 is determined by the changes of the shape of the model *DEM* with $T_{\rm M}$. In fact, if $T_{\rm M}$ is much lower than the temperature $T_{\rm max}$ of maximum abundance of the emitting ion, the model *DEM* is very low at temperatures where the $G_j(T)$ is non-negligible, resulting in a low value of $J_j(T_{\rm M})$ and a very high value of $R(T_{\rm M})$. When $T_{\rm M}$ approaches $T_{\rm max}$, the *DEM* value at the relevant temperatures rises quickly, thus lowering $R(T_{\rm M})$. For high values of $T_{\rm M}$ the model *DEM* is always non-negligible at temperatures where the $G_j(T)$ is greater, so that the changes in the $J_j(T_{\rm M})$ and $R(T_{\rm M})$ functions are more limited.

The value of $T_{\rm M}^\star$ determined from the crossing point is used to determine the loop-top temperature and the loop half-length using Eq. (27).

The loop top temperature is determined from Eq. (28) and can be compared with the results obtained with the emission measure analysis and line ratio techniques.

The value of p_0 can be determined from density and temperature measurements from line ratios, and is used to

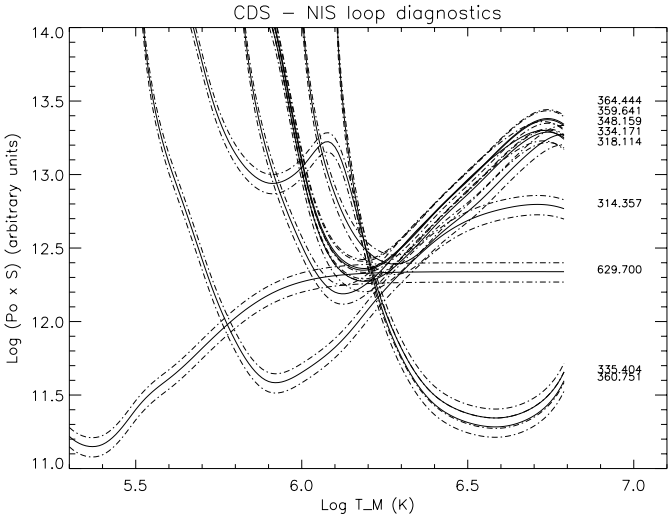

Fig. 6. Application of the loop diagnostic technique to a loop observed by the CDS instrument on board the SOHO satellite (from Paper II, Fig. 7).

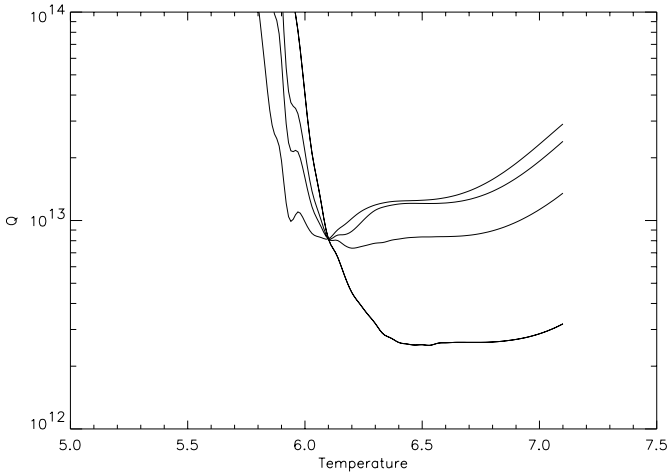

Fig. 7. Results of the diagnostic procedure applied to a simulated loop, with Log $T_{\rm M} = 6.1$ (T in K) and $Q = 8.3 \times 10^{12}$ g cm^{-3} s^{-2} K$^{1/2}$. The abscissa reports Log $T_{\rm M}$, the ordinate reports the quantity Q (given by Eq. (33)).

determine the loop maximum section $S_{\rm M}$ from the measured $p_0 S_{\rm M}$; the result can be compared with observations.

It is important to note that once the loop shape parameters ($S_{\rm M}/S_{\rm m}$, n) are chosen, the shape of the $R(T_{\rm M})$ functions is fixed because the loop *DEM* is completely defined. Changes in the values of $S_{\rm M}/S_{\rm m}$ and n have large effects on the evaluation of $J(T_{\rm M})$ for transition region lines, but cause more limited changes to $J(T_{\rm M})$ for the coronal lines. The values of $S_{\rm M}/S_{\rm m}$ and n are adjusted in order to obtain the best agreement between the $R(T_{\rm M})$ curves of the transition region and coronal lines.

In order to test the procedure a simulation has been performed using the following loop model parameters

- $T_{\rm M} = 10^{6.1}$ K,
- $N_{\rm e}T = 10^{15.2}$ cm^{-3} K,
- $S_{\rm M} = 2 \times 10^{18}$ cm^2.

These values are reasonably in agreement with the values derived from the observations (see Aschwanden et al. 1999, 2000a for comparison).

Four arbitrary iron lines sensitive to the temperature range from $10^{5.9}$ to $10^{6.9}$ have been used and the radiation emitted by the loop has been evaluated using Eq. (29). Line emissivities have been taken from the CHIANTI database (Dere et al. 1997, 2001; Landi et al. 1999). The procedure has been applied and the results are shown in Fig. 7. The absence of errorbars is obviously due to the fact that line intensities are simulated values.

All lines meet in a common crossing point, corresponding to the input temperature Log $T_{\rm M} = 6.1$ and

$$Q = \frac{S_{\rm M} p_0}{4k^2} \sqrt{\frac{A}{C}} \frac{1}{4\pi d^2} = 8.3 \times 10^{12}. \quad (33)$$

In the real case, the experimental uncertainties in the measured fluxes will appear as "stripes" and allow to identify a box of possible $(T_{\rm M}, Q)$ solutions, thus providing uncertainties in abscissae and ordinate of the crossing point. Example of this can be found in Fig. 6 and in Paper II (Figs. 7, 9, 11 and 13), where CDS observations are analyzed by means of this technique.

4. Discussion

Recent observations have clearly shown that a large part of the loops are nearly isothermal for most of their length, and for nearly all of their coronal section (Neupert et al. 1998; Aschwanden et al. 1999, 2000a; Lenz et al. 1999). These authors also point out that steady-state models based on the solution of the energy equation cannot reproduce this observational feature. In fact, previous attempts to fit observations using this kind of loop models have faced difficulties in obtaining sufficiently long isothermal regions (see Fig. 3a in Lenz et al. 1999, and Paper II).

Preliminary analysis performed by the authors (Landini et al. 1999) on CDS active regions has also shown that the observed temperatures, measured using line ratio techniques, are much more constant than predicted by the model. Also, some discrepancies between the observed and theoretical loop cross-sections were found; the top temperature values agreed only marginally. In Paper II these preliminary results are confirmed with a more careful analysis, indicating that the model alone, as it is now, is not able to account for the observed characteristics of the loops. This is consistent with the findings of Aschwanden et al. (1999, 2000a), showing that the RTV loop model, very similar in concept to the present one, is not able to reproduce the observations.

To understand why this discrepancy occurs, we have tried two different approaches:

1. We have added at the top of the model an isothermal region with the same section, pressure and

temperature of the top section of the model. This isothermal section allows us to simulate the realistic case of a nearly isothermal loop, and to calculate the expected total line flux;
2. We have released the assumption of thermal insulation at the base of the loop, by allowing $w(t_o)$ to assume any value (usual values are from 1 to 5).

4.1. The isothermal region on top of the loop

The problem of the interpretation of long isothermal regions on top of the loops has been addressed in several papers. In our simple model an isothermal solution can be obtained when power supply exactly balances radiative losses all over the region, although this may appear a rather unusual and ad hoc condition.

In the recent literature a number of different solutions have been proposed: these can be grouped in a few main types.

1. Reale & Peres (2000) suggest that the isothermal portion of an observed loop can be obtained by a bundle of parallel, static and hydrostatic filaments, modeled according to Serio et al. (1981) (RTV-like) assuming uniform heating along the loop length. When this bundle of loops is not spatially resolved, the observed temperature profile of the resulting structure can be flat. Unfortunately, several combinations of different loops in the bundle can yield the same temperature profile, so it is not possible to infer anything on each individual component;
2. Non-steady heating supply with suitable time intervals could mimic an isothermal loop, since the very effective conduction transfer will flatten the temperature profiles in very few thousand seconds, as suggested by Aschwanden et al. (1999, 2000a).
3. The Serio et al. (1981) model is able to reproduce the observed temperature profiles in case the heating is *not* uniform, but has a scale-height of $\simeq 17 \pm 6 \ \times 10^3$ km (Aschwanden et al. 2000b). A more complete study by Aschwanden et al. (2001) provide a revised scale-height value of $\simeq 12 \pm 5 \ \times 10^3$ km.

This last solution was proposed by Landini & Monsignori Fossi (1975). The suggested power supply can be put in the form

$$H = H_0 \ \mathrm{e}^{-\frac{h}{Kh_{\max}}} \tag{34}$$

where $h_{\max}$ is the maximum distance along the loop ($h_{\max} = L/2$) and K is a positive constant. With a proper choice of the constant K it is possible to obtain a quasi-constant heating function for part of the loop length, and a decrease for temperatures greater than T_{M}. An example is displayed in Fig. 8, where the energy balance between the radiative losses and the heating function is reported: both a constant and an exponential heating function are plotted to show that differences arise only at temperatures of the order of, or greater than T_{M}.

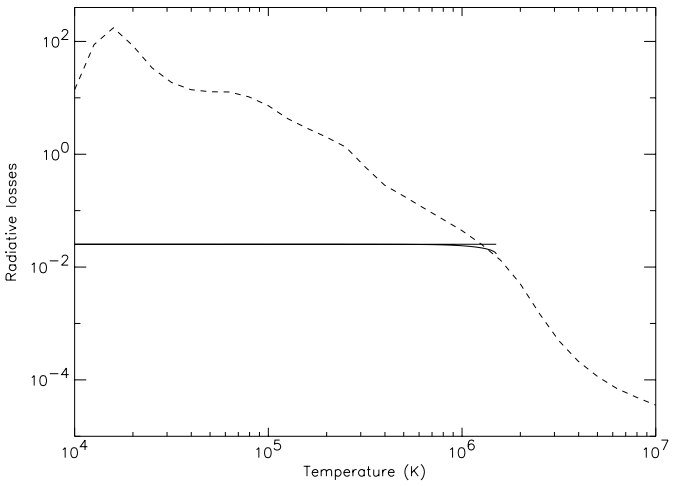

Fig. 8. Energy balance considering two different kinds of heating. Dashed line: radiative losses; full lines: two different kind of heating: uniform heating (constant function), and exponential heating (according to Eq. (34) with $K = 0.4$). These two different heating functions are nearly constant and differ significantly only for Log $T > 6.1$ (T in K).

Figure 8 shows that for $T > T_{\mathrm{M}}$, the difference $E_1 - E_{\mathrm{r}}$ is smaller in the case of exponential heating than it is for uniform heating and so, from Eq. (1), the conductive losses, E_{c}, are smaller. This leads to a smaller temperature gradient and a near-isothermal character to the loop top region. This is in agreement with our "semiempirical" model, that requires the somewhat arbitrary joining of a steady-state, hydrostatic loop model with an ad hoc isothermal region whose emission measure is chosen from the observed loop length, cross-section and electron density. A future paper will be devoted to a careful study of the consequences of such a heating function.

4.2. Conductive flux at the base of the loop

Oluseyi et al. (1999) obtained radiation-dominated loop models as a class of solutions of a quasi-static loop model where the boundary conditions at the interface between the chromosphere and the transition region are different from the RTV model, adopting the Fontenla et al. (1990, 1991, 1993) model for the conditions below 10^5 K. Oluseyi et al. (1999) find that the solutions matching the observations can be divided into three main classes, one of which requires the conductive energy to be negligible relative to the radiation energy, thus providing a long isothermal region.

Following this suggestion we have investigated the properties of models having large conductive fluxes at the base. The flux remains constant over large part of the temperature model (see Fig. 9).

The main results are that a very steep temperature gradient is obtained at the loop feet and a long flat temperature region is produced at the top. Both these results point in the right direction; but a much lower T_{M} value is

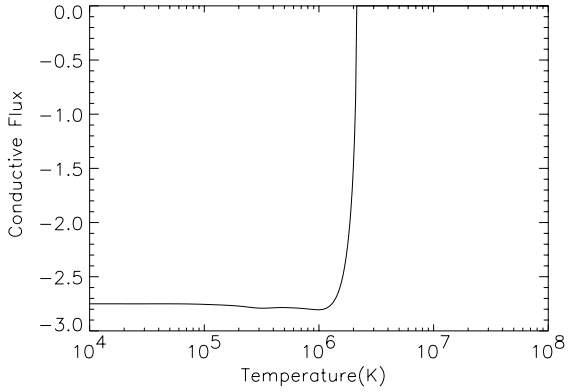

Fig. 9. The scaled conductive flux for non insulated loop; compare this figure with Fig. 3.

necessary to reach the same top coronal temperature; the scale length becomes too small unless very low pressure values are present.

However this model coupled with an isothermal coronal region may solve the problem as will be shown in Paper II.

5. Conclusions

In the present work the hydrostatic, steady-state loop model of Landini & Monsignori Fossi (1975) is developed:

- The effects of the geometry of the loop are taken into account including a variable loop cross-section. This can be important in order to reproduce the intensities of the transition region lines.
- A simple diagnostic technique is developed to compare model predictions with observations in order to a) check if the model agrees with observations, b) determine the main physical quantities of the loop.
- The presence of an an isothermal region at the top of the loop, suggested by Aschwanden et al. (1999, 2000a) following SOHO-EIT observations, is investigated, and the diagnostic procedure has been modified in order to take into account its presence. This isothermal portion is discussed in light of the (still unknown) heating function.
- We also discuss the model properties when non-negligible conductive flux at the base (non insulated loops) are assumed.

A comparison between the present loop model and observations is described in Paper II, where observations of active region loops from SOHO and Yohkoh satellites are analyzed: detailed plasma temperature, density and pressure diagnostics is used to constrain the loop model, and loop geometry is investigated from broad-band images and emission line intensity maps.

Acknowledgements. The authors acknowledge very useful discussions with Prof. S. K. Solanki, Dr. I. Rüedi, Dr. A. Brković and Dr. M. J. Aschwanden.

References

Aschwanden, M. J., Newmark, J. S., Delaboudinière, et al. 1999, ApJ, 515, 842
Aschwanden, M. J., Alexander, D., Hurlburt, N., et al. 2000a, ApJ, 531, 1129
Aschwanden, M. J., Nightingale, R. W., & Alexander, D. 2000b, ApJ, 541, 1059
Aschwanden, M. J., Schrijver, C. J., & Alexander, D. 2001, ApJ, 550, 1036
Brković, A., Landi, E., Landini, M., et al. 2002, A&A, 383, 661 (Paper II)
Dere, K. P., Landi, E., Mason, H. E., et al. 1997, A&AS, 125, 149
Dere, K. P., Landi, E., Young, P. R., & Del Zanna, G. 2001, ApJS, 134, 331
Fontenla, J. M., Avrett, E. H., & Loeser, R. 1990, ApJ, 355, 700
Fontenla, J. M., Avrett, E. H., & Loeser, R. 1991, ApJ, 377, 712
Fontenla, J. M., Avrett, E. H., & Loeser, R. 1993, ApJ, 406, 319
Kjeldseth-Moe, O., & Brekke, P. 1998, Sol. Phys., 182, 73
Landi, E., & Landini, M. 1999, A&A, 347, 401
Landi, E., Landini, M., Dere, K. P., et al. 1999, A&A, 135, 339
Landini, M., & Monsignori Fossi, B. C. 1973, A&A, 25, 9
Landini, M., & Monsignori Fossi, B. C. 1975, A&A, 42, 213
Landini, M., & Monsignori Fossi, B. C. 1981, A&A, 102, 391
Landini, M., Brković, A., Landi, E., et al. 1999, Space Sci. Rev., 87, 245
Lenz, D. D., De Luca, E. E., Golub, L., et al. 1999, ApJ, 517, L155
Neupert, W. N., Newmark, J., Delaboudinière, J.-P., et al. 1998, Sol. Phys., 183, 305
Ogawara, Y., Takano, T., Kato, T., et al. 1991, Sol. Phys., 136, 1
Oluseyi, H. M., Walker, A. B. C. II, Santiago, D. I., et al. 1999, ApJ, 527, 992
Orlando, S., Peres, G., & Serio, S. 1995a, A&A, 294, 861
Orlando, S., Peres, G., & Serio, S. 1995b, A&A, 300, 549
Peres, G., 1997, Proc. 5th SOHO Workshop, ESA SP-404, 55
Reale, F., & Peres, G. 2000, ApJ, 528, L45
Reale, F., Peres, G., Serio, S., et al. 2000a, ApJ, 535, 412
Reale, F., Peres, G., Serio, S., et al. 2000b, ApJ, 535, 425
Rosner, R., Tucker, W. H., & Vaiana, G. S. 1978, ApJ, 247, 686
Serio, S., Peres, G., Vaiana, G. S., et al. 1981, ApJ, 243, 288
The solar Maximum Mission Experiments, 1980, Sol. Phys., 65, 5
Spadaro, D., Lanzafame, A. C., Consoli, L., et al. 2000, A&A, 359, 716
Spitzer, L. 1962, Physics of Fully Ionized Gases (New York: Interscience), 144